Energy 174 (2019) 625–637

Contents lists available at ScienceDirect

Energy

journal homepage: www.elsevier.com/locate/energy

Kalina power plant part load modeling: Comparison of different approaches to model part load behavior and validation on real operating data

Fabian Dawo [a, *], Christoph Wieland [a], Hartmut Spliethoff [a, b]

[a] Institute for Energy Systems, Technical University of Munich, Boltzmannstr. 15, 85748, Garching, Germany
[b] ZAE Bayern, Abteilung 1 Technik für Energiesysteme und Erneuerbare Energien, Walther-Meissner-Str. 6, 85748, Garching, Germany

ARTICLE INFO

Article history:
Received 27 April 2018
Received in revised form
22 January 2019
Accepted 24 February 2019
Available online 25 February 2019

Keywords:
Kalina cycle
Off-design
Part load behavior
Modeling
Operating data
Geothermal

ABSTRACT

Geothermal energy can play a vital role in the mitigation of climate change due to its CO_2-neutral, renewable and non-fluctuating character. Because of the expensive preparation of the geothermal wells, the thermal water should be utilized with the highest efficiency. Therefore, the wells are often exploited in combined heat and power concepts. Consequently, the power plant operates in part load most of the time. However, this high portion of part load operation is often not fully considered in the design stage of the plant, due to a lack of suitable simulation models. Therefore, the purpose of this paper is to compare several approaches to simulate the part load behavior of the geothermal Kalina power plant in Unterhaching (Germany) and to validate them with operational data. Simulation approaches to calculate the isentropic efficiency of the turbine and the heat transfer coefficients of the heat exchangers are studied and compared on component level. An investigation of different combinations of these component models then follows. The results show that a detailed correlation to model the isentropic efficiency of the turbine is necessary to achieve sufficient accuracy. Furthermore, modeling plate heat exchangers with a power law approach for the heat transfer coefficient appears promising.

1. Introduction

In several areas in Germany, it is possible to exploit geothermal energy, which is a renewable energy source. Currently, there are nine geothermal power plants in operation with an installed capacity of about 40 MW, which produced 174.21 GW h of electricity in 2016 [1,2]. The economic potential of hydrothermal geothermal sources in Germany has been estimated by Eyerer et al. [3] to a total of 8700 TW h. This value is calculated taking the governmental subsidies of 25.2 cts/kWh into account. Utilizing this potential in a sustainable way results in an annual production of 8.7 TW h of electricity per year and the potential to operate more than 430 plants [3]. These numbers show that there is great expansion potential for geothermal power plants in Germany in the future.

Due to the low temperature level, the most commonly used technology to generate power from geothermal energy is the Organic Rankine Cycle (ORC). Several options are being investigated with the aim of optimizing and improving the ORC process. For example, multi-pressure systems, transcritical and supercritical cycles and zeotropic mixtures as working fluid. The goal of these optimizations is to find a perfect match between heat source, environmental boundary conditions, and the thermodynamic cycle.

Another promising technology to generate power from low enthalpy sources is the Kalina cycle (KC) process. The Kalina cycle utilizes an ammonia-water mixture as working fluid. These two components form a zeotropic mixture, which is advantageous in heat transfer because the evaporation does not take place isothermally. This reduces exergy destruction during heat transfer and enables efficiency gains over the ORC process. Several approaches to compare the KC with the ORC can be found in literature. Zhang et al. [4] provides a broad literature review of the research on the KC, including the comparison with the ORC and different correlations for calculating thermodynamic properties of ammonia-water mixtures. Rodriguez et al. [5] estimate a net power increase of 18% for the KC compared to a simple ORC at a thermal water temperature of 100 °C, they suggest the KC for low temperatures as an alternative to the ORC. Köhler [6] examined geothermal power plants for a thermal water temperature range between

* Corresponding author.
E-mail address: fabian.dawo@tum.de (F. Dawo).

https://doi.org/10.1016/j.energy.2019.02.173
0360-5442/

100 °C–200 °C and concluded that the KC with air cooling is advantageous in the lower temperature range. Although the KC extracts less energy from the thermal water than the ORC, it uses it more efficiently. Thorin [7] determines higher electrical power output for KC in industrial waste heat utilization. DiPippo [8] compares the operating data of geothermal power plants in operation and identifies a slightly better performance (3%) of the KC compared to the ORC processes. Walraven et al. [9] compare various ORC processes and the KC to generate electricity from geothermal sources. They conclude that the KC is comparable to the best ORC designs (transcritical or multi-pressure subcritical) if the thermal water exit temperature is limited. The papers discussed here show that the KC can be advantageous for low temperature levels as they occur in geothermal applications.

Projects using geothermal energy are often combined heat and power concepts, because these concepts are favorable in terms of preventing harmful CO_2 emissions and they offer economic benefits due to a higher number of full load operation hours of the plant [10]. Further information about determining the global warming impact of geothermal energy production by means of a life cycle assessment can be found in [11]. Most of these plants are heat-controlled, which means that they always provide the heat needed for e.g. district heating and use the excess geothermal energy to generate power. The high heat demands in wintertime cause the power plant to only operate in part load or being completely shut down. In summertime, the lower heat demand enables full load operation. However, the higher ambient temperatures, which define the heat sink of the plant, cause higher condensation pressures and thus lower power production by the plant. This behavior is shown exemplary in Fig. 1 for the Kalina power plant in Unterhaching (Germany) in 2016 by means of the fraction of the brine mass flow, which is available for power production. This power plant is integrated into a parallel combined heat and power concept, where the geothermal mass flow is separated into two streams. The first stream is controlled to provide enough energy to satisfy the demand of the district heating network. The remaining mass flow is utilized to generate power in the KC. Due to the high proportion of part load operation during the year, the part load behavior should be given high priority in the power plant design for combined heat and power systems.

Several approaches to simulate the part load behavior of power plants are described in the literature. Gabbrielli [12] proposes a design approach for binary geothermal power plants utilizing a detailed off-design performance model in order to evaluate the optimal design point of the power plant. He suggests a widely used correlation for the isentropic turbine efficiency in part load conditions. Jüdes et al. [13] describe the optimization of cogeneration plants using mixed-integer nonlinear programming and implement an empirical correlation to calculate the part load behavior of the steam turbine. This study compares different modeling approaches on the part load behavior of geothermal power plants. A description of the part load models examined in this paper is provided in Section 5. A detailed model of the KC in Unterhaching (Germany) is designed in *AspenPlus* [14] and *Matlab* [15] and validated with actual operating data. This model is then compared to several approaches described in the literature that are used to simulate part load behavior. The modeled part load behavior is finally used to estimate the annual power yield of the plant. This way, the novel part load model developed in this study is compared to the current state-of-the-art part load models found in the literature, in order to analyze the improved modeling.

This paper addresses to researchers and scientists in modeling power plants and energy providers, which operate or design power plants that mostly operate in part load conditions. This is the case for many CHP projects in the geothermal energy sector.

2. The Kalina cycle – process layout

The Kalina cycle was introduced in the early 1980s as a new thermodynamic power cycle using ammonia-water mixtures as working fluid [16–18]. Fig. 2 a) illustrates the process scheme of the KC power plant in Unterhaching (Germany). Fig. 2 b) shows the temperature-enthalpy process chart of the process. This plant has been successfully producing electricity since 2008 [19] and was the first KC power plant in Germany. The geothermal brine transfers energy to the ammonia-water working mixture in the evaporator (A-B). Thereby the basic solution, which contains 89 ma-% ammonia and 11 ma-% water, is partially evaporated (2–3). The working fluid mass flow is controlled in order to reach a temperature of 119.8 °C at the evaporator outlet, which corresponds to a vapor quality of approx. 0.94. Due to the higher boiling point of ammonia as compared to water, this two-phase mixture can then

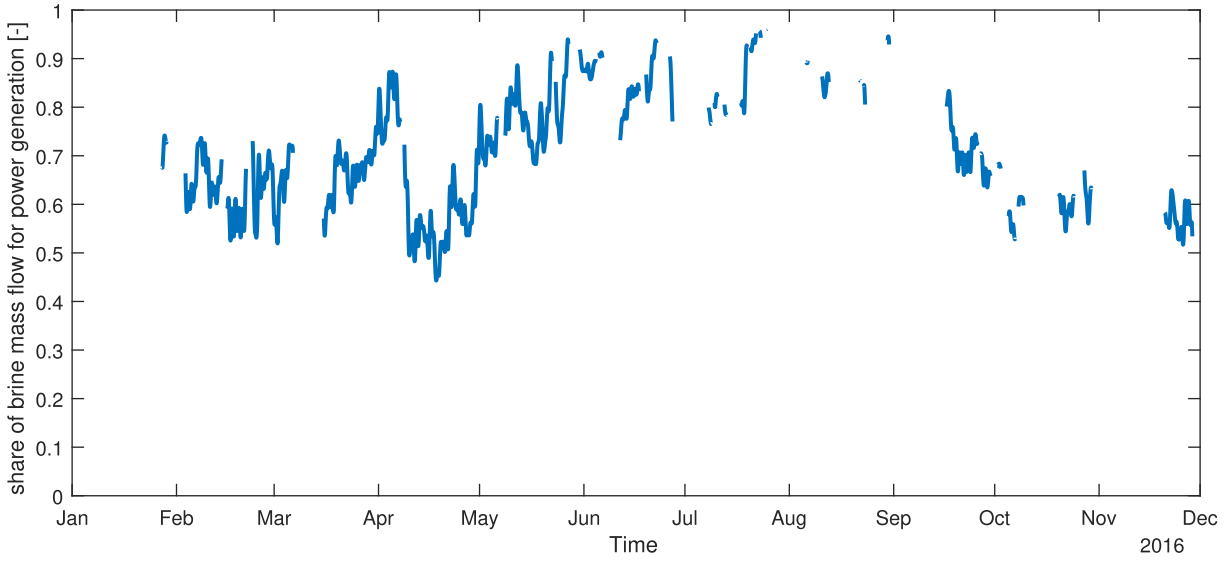

Fig. 1. Fraction of full load operation in 2016 for the Kalina power plant in Unterhaching (Germany).

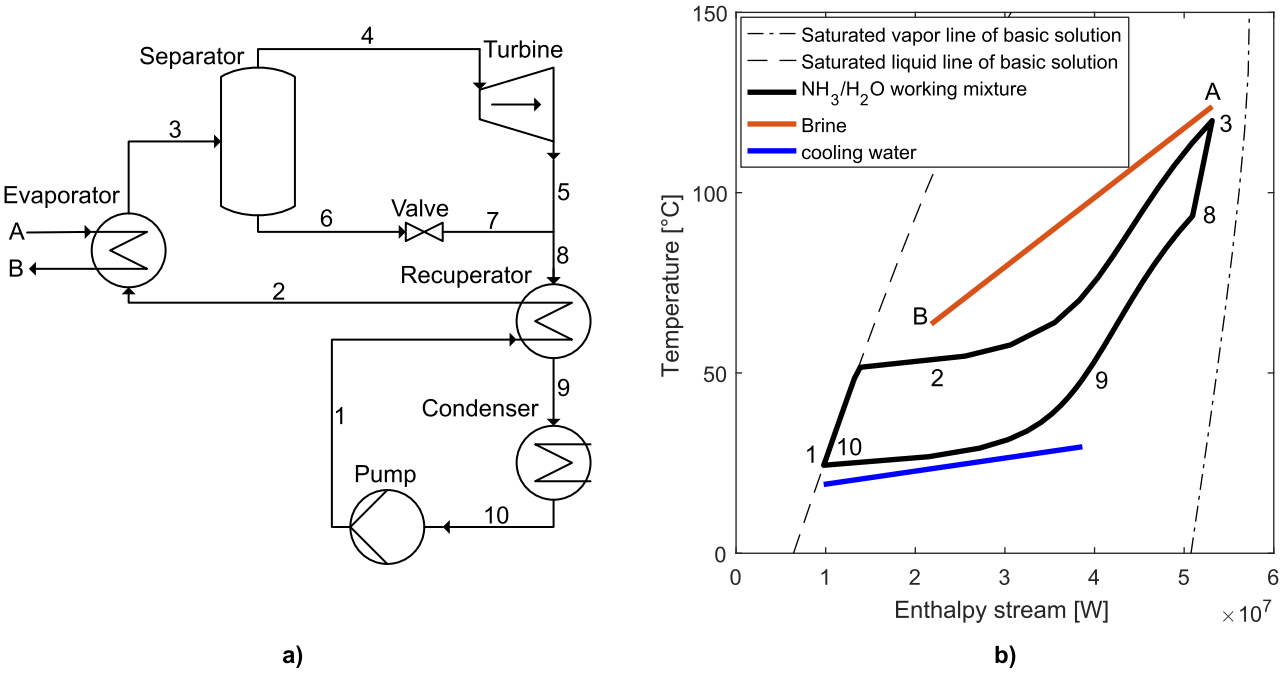

Fig. 2. a) Process scheme of the KC power plant in Unterhaching (Germany); b) Temperature-enthalpy process chart of the KC.

be separated in an ammonia-poor liquid phase (6) and an ammonia-rich vapor phase (4) in the separator. The vapor stream expands in the turbine to the lower pressure level of the cycle (5) and is then mixed with the ammonia-poor liquid stream (7), which has been expanded to the same pressure by a throttle valve. In the next step, the internal recuperator recovers a part of the sensitive heat from (8) to (9) before the working mixture is condensed (10). The coolant used is water from a wet cooling tower. The fluid circulation pump then compresses the liquid working fluid to the high pressure level of the cycle (1). In the last step, the fluid is preheated in the recuperator to state (2) and flows back into the evaporator to close the cycle.

Fig. 2 b) shows the temperature-enthalpy diagram of the process, displaying only the states of the basic solution, therefore states 4, 5, 6, 7 are omitted for the sake of clarity because the mixture composition is different in these states and the saturation lines of the diagram are not valid for these compositions. The figure also illustrates the major advantage of the KC over the ORC: the non-isothermal evaporation of the zeotropic working fluid mixture (2–3). Due to the good adaptation of the temperature profiles on the heat source and the sink, exergy destruction is reduced during heat transfer. Table 1 summarizes the main design parameters and component types of the power plant.

Table 1
Main design parameters and component types of the power plant.

Thermal water	
Temperature	122 °C
Pressure	9 bar
Volume flow	140 l/s
Process parameters of the power plant	
Nominal power	3,36 MW
Live steam temperature	119.2 °C
Live steam pressure	19 bar
Condensing pressure	6.8 bar
Components of the KC	
Turbine	Single stage radial turbine
Heat exchanger type	Plate heat exchangers
Cooling system	Wet cooling tower

3. Preparation of operating data

This study utilizes the operation data of the Kalina power plant in Unterhaching (Germany) from 2016. The data of the power plant, the district heating network, and the geothermal water pump were recorded and stored for 884 different measuring points. To validate the different models described in this paper, data in 15-min time steps is used for the entire year of 2016. Since the power plant only operates at full load in the summertime, the operation in the design state defined in Table 1 never occurs, due to the higher ambient temperatures, which result in higher condensation pressures and lower power output (see Fig. 1). Therefore, the maximum operating point is determined from the power plant operation data. The methodology is as follows: The complete dataset is examined for times at which several important operating parameters differ by a maximum of 5% of the corresponding maximum value. The operating parameters considered here were the pressure after the fluid circulation pump (1), the power output of the turbine, the temperature after the evaporator (3), the brine volume flow (B), the working mixture volume flow after the fluid circulation pump (1), and the condensation pressure (9) (the indication of the states corresponds to Fig. 2 (a)). The measured values are then averaged over time to obtain the maximum operating point (see Table 2).

It should be mentioned at this point that the measured data is partly inconsistent. For example, the transferred heat from the hot

Table 2
Process parameters for the maximum operating point in 2016.

Power output	2364 kW
Live steam temperature	119.98 °C
Live steam pressure	18.7 bar
Condensing pressure	8.6 bar
Working mixture mass flow	29.2 kg/s
Turbine mass flow	28.42 kg/s
Brine mass flow	121.7 kg/s
Brine inlet temperature	123.9 °C
Brine inlet pressure	9.1 bar

side of the evaporator does not match the absorbed heat on the working medium side. This is probably the result of a combination of measurement uncertainties related to the measuring devices and difficulties in taking measurements within the thermal water circuit, due to problems like scaling [20]. In addition, the enthalpy of the ammonia-water mixture is very sensitive to changes in pressure and temperature in the two-phase region, which leads to rather substantial uncertainties in the calculated enthalpy with only slight measurement uncertainties.

4. Process model and calculation of the annual power yield

4.1. Process model and relevant assumptions

This section provides a detailed description of the novel designed model for the KC in Unterhaching (Germany). A special focus is put on the simulation of the part load behavior of the power plant. The KC was modeled with the commercial Software *Aspen-Plus V8.8* [14], utilizing *Aspen Exchanger Design and Rating* (EDR) to model the detailed geometry of the evaporator and the recuperator. Since the fluid circulation pump has only a small influence on the overall process, it is modeled with a constant isentropic efficiency of 0.8. The plate heat exchangers (evaporator and recuperator) are modeled by utilizing their detailed geometry, such as the number of channels for the hot and the cold side, horizontal and vertical dimensions of the plate, plate thickness, compressed plate pitch, number of plates and the chevron angle, within the EDR tool. The EDR tool is able to calculate pressure drop, heat exchanger duty, overall heat transfer coefficient, outlet temperatures, and several other values for part load conditions. The separator separates the vapor and liquid phases of the partially evaporated working mixture after the evaporator. It is assumed to be adiabatic and operates isothermally at the evaporator outlet temperature with no pressure drop. The following valve then throttles the liquid stream isenthalpic to the turbine outlet pressure. The vapor stream expands to the condenser pressure in the turbine. In order to model the part load behavior of the turbine, the following empirical correlation was derived from the operational data:

$$\eta_{s,T} = \eta_{s,T,MP}\left[a_{00} + a_{10}\cdot\left(\frac{\dot{m}}{\dot{m}_{MP}}\right) + a_{01}\cdot\left(\frac{p_9}{p_{9,MP}}\right) + a_{20}\cdot\left(\frac{\dot{m}}{\dot{m}_{MP}}\right)^2 + a_{11}\cdot\left(\frac{\dot{m}}{\dot{m}_{MP}}\right)\cdot\left(\frac{p_9}{p_{9,MP}}\right)\right] \quad (1)$$

With $a_{00} = -0.0429; a_{10} = 1.781; a_{01} = 0.2718;\ a_{20} = -0.5579; a_{11} = -0.4609$ and the isentropic efficiency at the maximum operation point $\eta_{s,T,MP} = 0.6618$ This correlation defines the isentropic efficiency of the turbine as a function of the ratio between actual and maximum operation point values of working fluid mass flow and condensation pressure. It was derived from the operating data from 2016. The root-mean-square deviation (RMSD) is 0.011 and is calculated as follows:

$$\mathrm{RMSD} = \sqrt{\frac{\sum_{i=1}^{n}(y_{data} - y_{model})^2}{n}} \quad (2)$$

Fig. 3 illustrates the good fit between the modeled isentropic efficiency of the turbine and the one calculated from measurements. The isentropic efficiency is calculated by the specific enthalpies in state (4) and (5) and the theoretically achievable enthalpy in state (5) for an isentropic expansion:

$$\eta_{s,T} = \frac{h_4 - h_5}{h_4 - h_{5,s}} \quad (3)$$

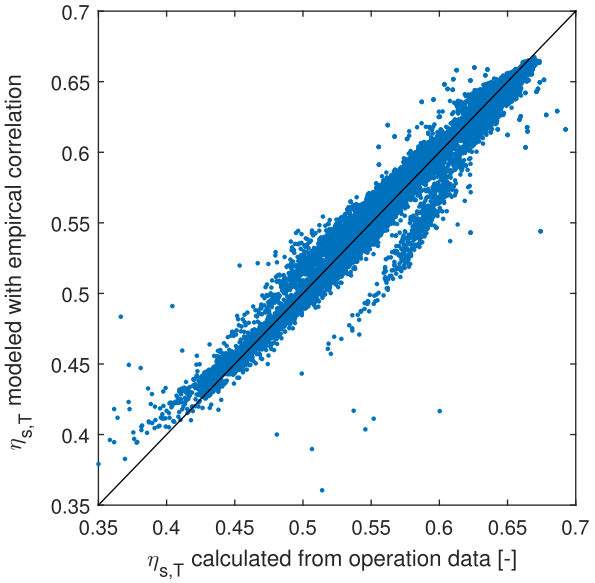

Fig. 3. Comparison between isentropic efficiency calculated from the measured operation data and calculated from the developed correlation.

The enthalpies at state (4) and (5) are determined with the measured operational data: the temperature at state (4) T_4, the measured pressure at state (4) p_4 and (5) p_5, the working fluid mass flow in the turbine $\dot{m}_4$ and the power output of the turbine P_T.

$$h_4 = h(T_4, p_4)$$

$$h_5 = h_4 - \frac{P_T}{\dot{m}_4}$$

$$h_{5,s} = h(p_5, s_4)$$

Since the electrical power output of the KC plant is used for the calculation of the isentropic efficiency mechanical losses and generator losses are also taken into account by the isentropic efficiency defined in equation (3). After the turbine, the two separated streams are reunited in the mixer and flow through the recuperator to the condenser. The condenser fully condenses the working fluid to saturation state. A detailed modeling of the cooling circuit is omitted, since the wet cooling towers are not controlled and operated independently of the operating point. The pressure losses in the mixing point and the condenser are set to the values of the maximum operating point. Table 3 summarizes them. There are two controlled variables in the model. The working fluid mass flow is adjusted in order to set the temperature at the evaporator outlet to the value of the maximum operating point, as in the control mechanism of the real power plant. In addition, the fluid circulation pump outlet pressure is manipulated to set the live steam pressure to the value of the maximum operating point. Boundary conditions

Table 3
Measured pressure losses of the maximum operating point for the components.

Component	Pressure loss [bar]
Mixing point	0.1705
Condenser	0.0597
Recuperator hot side	0.23
Recuperator cold side	0.3091
Evaporator hot side	0.6832
Evaporator cold side	1.342

of the process simulation are the brine inlet conditions (temperature, pressure, mass flow) and the condensation pressure. The condensation pressure is used as a boundary condition instead of the ambient temperature because it is closer to the process.

4.2. Methodology to calculate annual power yield

The previous section described the general model to determine the part load behavior of the KC plant. The annual power yield is now calculated with this model by the following methodology. Therefore, the condensation pressures occurring during 2016 are discretized into six levels. Fig. 4 a) shows these condensation pressure levels. The lowest level contains all pressures below 5.5 bar, the highest all pressures over 9.5 bar. In between, the levels are divided equidistantly in 1 bar steps. Subsequently, the power output of the turbine is calculated for all pressure levels while varying the brine mass flow. The modeled relation between brine mass flow and turbine power output is then fitted with a third-degree polynomial for every condensation pressure level as a function of the brine mass flow. Fig. 4 c) illustrates the fit between turbine power output and brine mass flow exemplarily for three pressure levels. The figure also shows the corresponding measured turbine power output for the illustrated pressure levels. A good match between model and operating data can be observed. This figure also illustrates the general distribution of the operating points depending on the boundary conditions. With increasing condenser pressure (increasing ambient temperature) the turbine power decreases. For an increasing brine mass flow (decreasing heat demand in the district heating network) the power output rises. In the last step, the turbine power is calculated for every time step of 2016. Therefore, the appropriate fit function (depending on the corresponding condensation pressure level) is used to

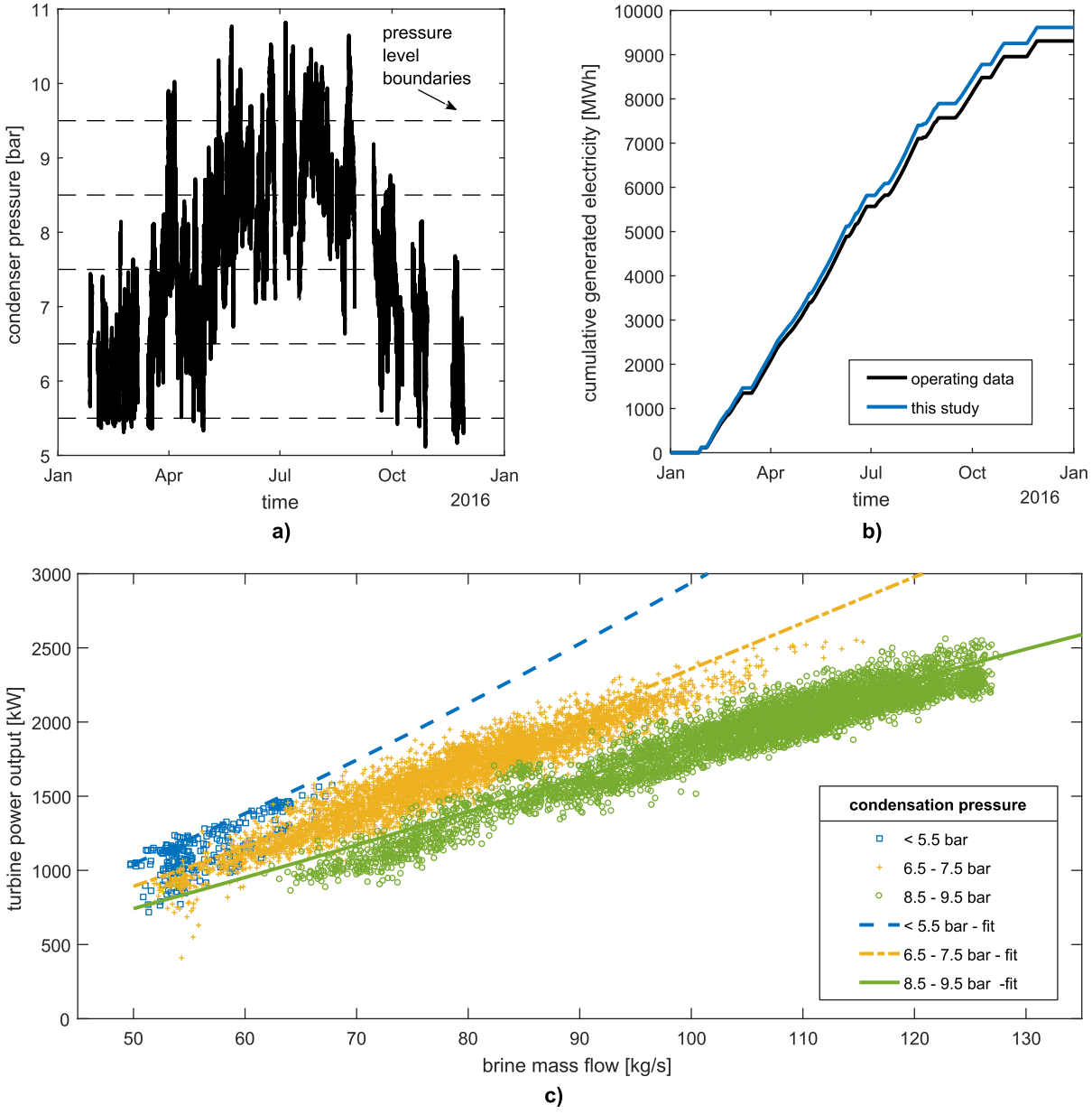

Fig. 4. Methodology to model the annual power yield. a): Condensation pressure in 2016 with pressure levels (dashed lines). b) Comparison of model and operating data for the cumulative power in 2016. c) Fit between brine mass flow and turbine power output for exemplarily chosen pressure levels.

determine the power output as a function of the current brine mass flow. This power is considered to be constant for the individual time steps and used to calculate the annual power yield. Fig. 4 b) shows the modeled cumulative power output over the year 2016 and compares it with the measured operating data. The comparison shows a good match between model and data.The model only slightly overestimates the power output. While the annual yield of the power plant in 2016 was approximately 9.31 TW h, the model calculates a power yield of 9.62 TW h, which corresponds to a deviation of about 3%. The good agreement between model and operating data leads to the conclusion that the model depicts the part load behavior with sufficient accuracy. This model will be used as a reference to evaluate several literature approaches to simulate part load behavior.

5. Approaches used in the literature to simulate part load behavior and definition of studied models

Several attempts to simulate part load behavior of power plants can be found in the literature. In the KC process, the turbine and the heat exchangers mainly determine part load behavior, which is why this paper focuses on these components.

5.1. Turbine part load behavior

Gabbrielli [12] evaluates the isentropic turbine efficiency in part load conditions with the following formula:

$$\eta_{s,T} = \eta_{s,T,D} \sin\left[0.5\pi\left(\frac{\dot{m}}{\dot{m}_D}\cdot\frac{\rho_{in,D}}{\rho_{in}}\right)^{0.1}\right] \quad (4)$$

The subscript D marks the design conditions. Several authors use this equation to calculate the off-design behavior of turbines in power plant simulations [21–23].

Jüdes et al. [13] present another approach to calculate the isentropic efficiency of steam turbines in part load conditions. They developed an empirical correlation of the isentropic efficiency as a function of the ratio of actual mass flow and design mass flow:

$$\eta_{s,T} = \eta_{s,T,D}\cdot\left[-1.0176\left(\frac{\dot{m}}{\dot{m}_D}\right)^4 + 2.4443\left(\frac{\dot{m}}{\dot{m}_D}\right)^3 - 2.1812\left(\frac{\dot{m}}{\dot{m}_D}\right)^2 + 1.0535\left(\frac{\dot{m}}{\dot{m}_D}\right) + 0.701\right] \quad (5)$$

This efficiency has to be corrected for part load conditions where the outlet steam quality differs from the design conditions by the following equation:

$$\eta_{s,T,corr} = \eta_{s,T} - 0.5\cdot x_e \quad (6)$$

Fig. 5 compares the three different approaches to model the isentropic efficiency of turbines in part load conditions by means of a parity plot. The model developed in this study achieves the best agreement with the operating data with an RMSD of 0.011. The empirical correlation in Jüdes et al. [13] does not quite match the data as well. The RMSD for this approach is 0.073. The largest deviation between model and operating data results for the approach based on Gabbrielli [12] with a RMSD of 0.099.

Another widely used approach for modeling part load behavior of steam turbines is Stodola's ellipse law [12,13,21–23]. It links turbine outlet and inlet pressure and mass flow through the turbine and is valid for uncontrolled multistage expansion turbines to high vacuum [24,25]:

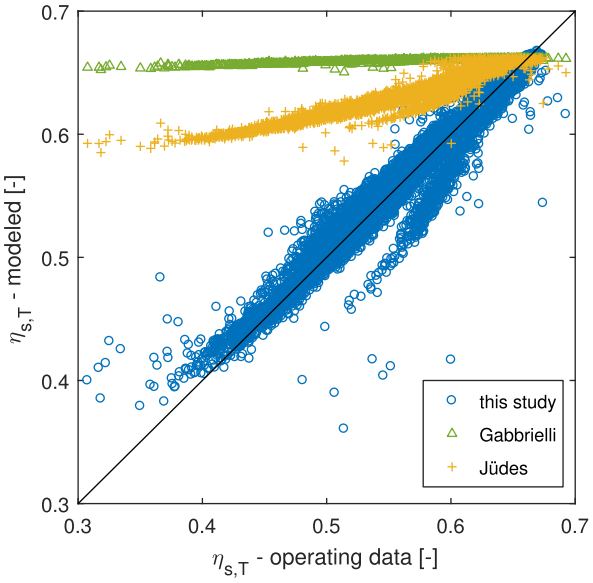

Fig. 5. Comparison of three approaches to model the isentropic efficiency at part load conditions.

$$p_{out} = \sqrt{p_{in}^2 - \left(\frac{\dot{m}}{\dot{m}_D}\right)^2\left(p_{in,D}^2 - p_{out,D}^2\right)} \quad (7)$$

If the inlet and outlet pressure as well as the mass flow at one operating point are known (e.g. at design conditions), one of the three dependent variables can be calculated with the help of the other two.

All these suggested correlations for the part load behavior of turbines have in common, that they do not require any geometric data of the turbine itself and therefore can be used even if the detailed design of the turbine is unknown. If the geometry is known, more sophisticated models for the turbine part-load behavior are viable. Fuhaid et al. [26] predicted the off-design performance of a radial inflow turbine and validated their model with experimental data. Du et al. [27] did a study on control approaches for the Kalina cycle utilizing a radial-inflow turbine with variable nozzles. They evaluated the performance of the cycle with a detailed part load model of the turbine. Fiaschi et al. [28] discussed the off-design performance of radial turbo-expanders for ORC applications for several working fluids with a zero-dimensional model for the design of the turbine. Another radial-inflow turbine for ORC systems is investigated by Song et al. [29]. They proposed a one-dimensional analysis method to describe the off-design performance of the turbine. Zheng et al. [31] utilized another one-dimensional model for the design and off-design performance of a radial-inflow turbine and also did 3D CFD steady state simulations of the turbine.

In general, it is very important to check the validity of the utilized correlations. Usually these correlations are valid for a very specific turbine type and working fluid. Unfortunately there is a lack of accessible correlations for the part load operation of some turbine types. Therefore, in many cases a not perfectly matching correlation has to be chosen.

5.2. Heat exchanger modeling in part load conditions

For heat exchanger modeling, three different approaches were

chosen. The first approach is the above-mentioned detailed modeling in *Aspen Exchanger Design and Rating* (EDR), which is also utilized by [12]. The second method is the definition of constant overall heat transfer coefficients (ohtc) for the different heat exchangers [10,30], and the third approach is the implementation of heat transfer coefficients as a function of mass flow. The commercial thermodynamic cycle simulation software *EBSILON Professional* [32] also uses this approach. Therefore, the ohtc and the mass flow at the design point (or any other operating point) need to be known. The ohtc at part load conditions is then easily computed with the following power law equation:

$$U = U_D \cdot \left(\frac{\dot{m}}{\dot{m}_D}\right)^a \tag{8}$$

This study utilizes the working fluid mass flow in equation (8) because it is assumed that measurements uncertainties are smaller in the power cycle than in the brine mass flow, since there is no scaling. Yoon et al. [23] use this approach with an exponent a of 0.8. This exponent is derived from the Dittus-Boelter correlation [33] and is valid for pipe flow. Therefore, this approach is able to simulate shell and tube heat exchangers very well. To obtain a better match between operating data und model for the plate heat exchangers in the power plant in Unterhaching (Germany), the exponent a was fitted to 1.12 for the evaporator and 1.16 for the recuperator by using the operating data. Fig. 6 shows the plots for the power law approach with the exponent from literature and the exponent from this work and the operating data. The ohtc was determined with the logarithmic mean temperature difference (LMTD) concept [34]:

$$\Delta T_{lm} = \frac{\Delta T_A - \Delta T_B}{\ln\left(\frac{\Delta T_A}{\Delta T_B}\right)} \tag{9}$$

$$U = \frac{\dot{Q}}{\Delta T_{lm} \cdot A_{ex}} \tag{10}$$

The logarithmic mean temperature difference is the logarithmic average of the temperature differences between the two ends of a heat exchanger (A and B). The ohtc is then calculated with the exchanger duty $\dot{Q}$ and the heat exchanger area A_{ex}. However, this approach to compute the ohtc is only an approximation, due to the non-linear temperature gradient of the ammonia-water mixture during heat transfer (see Fig. 2 b)) [35].

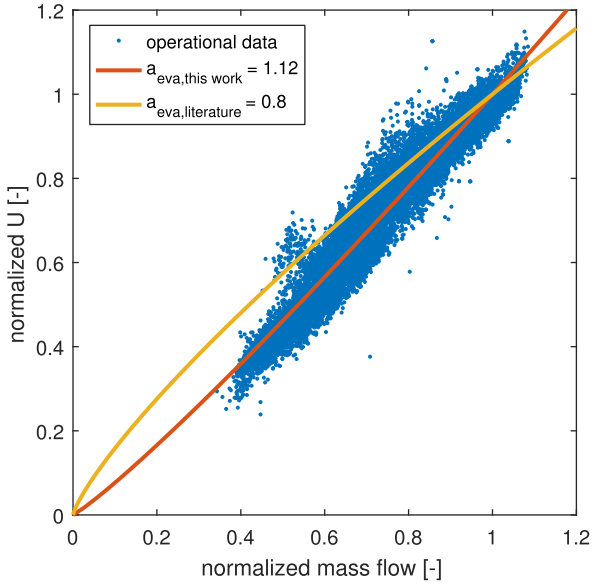

Fig. 6. Comparison of the different exponents for the power law approaches to model heat exchangers for the evaporator.

Fig. 7 compares the four approaches to simulate the part load behavior of heat exchangers. The results for the ohtc, the LMTD, and the heat exchanger duty are exemplarily shown for varying heat source mass flows in the evaporator. The working fluid mass flow is chosen to set the outlet temperature on the cold side to 119.98 °C. The inlet conditions are the same as in the maximum operating point and the values of the EDR modeling at this operating point are used to calculate the normalized values plotted in Fig. 7. The figure shows that the calculated transferred heat barely differs for the four considered approaches and that the duty declines with declining mass flow as expected. For the mean temperature difference and the heat transfer coefficient, a different picture emerges. The EDR approach results in the highest LMTD because the other approaches underestimate this value systematically due to the non-linear temperature profile. This underestimation is compensated with a higher calculated ohtc in the power law and constant ohtc approach, with the result that the transferred heat hardly differs. Another aspect worth mentioning is that for all approaches except the fitted power law with increasing part load (decreasing heat source mass flow), the heat exchanger performance seems to increase (decreasing LMTD).

5.3. Definition of studied model combinations

The different modeling approaches described in the previous section, are divided into three groups: isentropic turbine efficiency, turbine outlet pressure, and heat exchanger models. Based on these three groups and the above-mentioned different approaches, five combinations of the respective approaches are defined to form a corresponding part load model of the power plant (see Table 4). The model in the first column is the one developed in this study (see Section 4). The design point model utilizes the constant values of the maximum operating point for the isentropic efficiency, the turbine outlet pressure, and the heat transfer coefficients for every operating point. The literature model uses the equation of Gabbrielli [12] to model the isentropic turbine efficiency, Stodola's ellipse law to compute the turbine outlet pressure, and the power law approach to calculate the overall heat transfer coefficient in part load conditions with the exponent $a = 0.8$ from the literature. Model-4 and Model-5 are intended to illustrate the difference between the constant turbine outlet pressure and the pressure levels approach, which was described in Section 4.2. Therefore, both apply the isentropic turbine efficiency model developed in this study and use the improved power law for heat transfer coefficient calculation ($a = 1.12$). The EDR tool is not used for these two models for three reasons: First, the difference between the EDR and the improved power law approach can be illustrated by this methodology by comparing the model in this study and Model-5. Second, the approach is numerically very expensive and convergence problems occur regularly. Third, the detailed geometry of the heat exchangers is needed to use this approach, which often is not available. Jüdes [13] approach is not investigated further because it is similar to the approach used in this study and results in a poorer agreement with the operating data because the turbine outlet pressure is not considered.

6. Validation for several operating points

As a first step, the defined models are validated with several stationary operating points. Table 6 in the appendix section

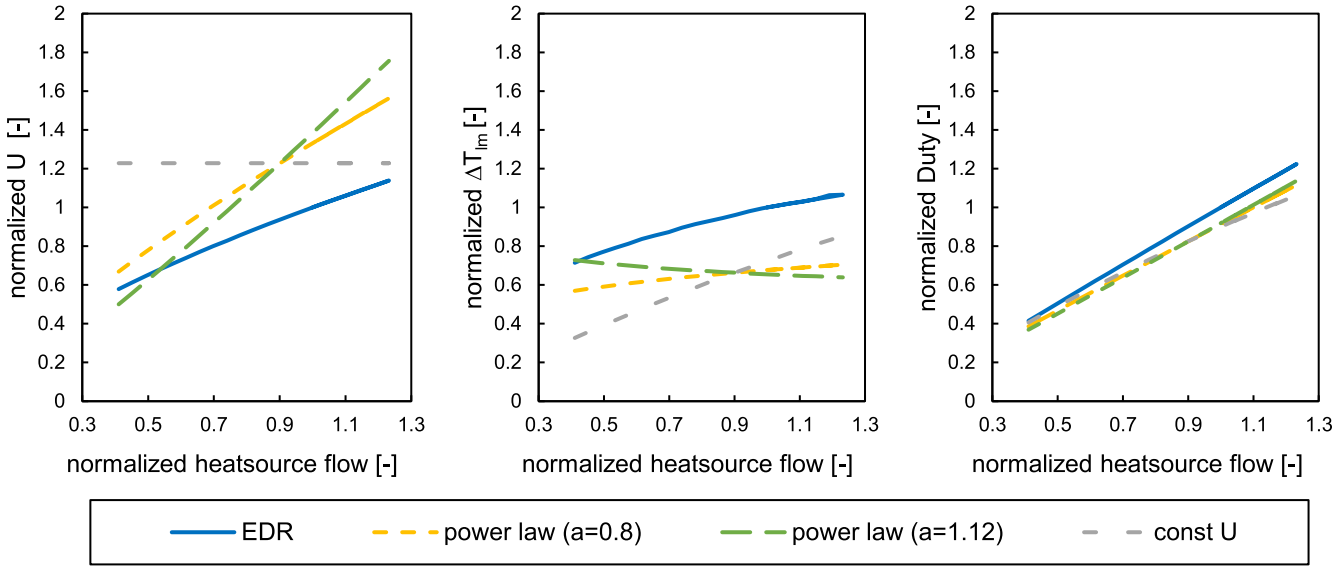

Fig. 7. Comparison of the different approaches to model heat exchangers for the evaporator.

Table 4
Classification of the described model approaches and definition of the studied combinations for the part load model of the plant.

	Model in this study	Design point model	Literature model	Model-4	Model-5
Isentropic turbine efficiency					
This study	X			X	X
Constant		X			
Gabbrielli			X		
Jüdes					
Turbine pressure outlet					
Pressure levels	X				X
Constant		X		X	
Stodola			X		
Heat exchanger models					
EDR	X				
Constant U		X			
Power law (literature)			X		
Power law (fit)				X	X

summarizes the operating data, the RMSD and the MAPE for all five part load models for gross power, working fluid mass flow, and the temperatures and pressures at the different plant locations defined in Fig. 2. T_5, T_7 and p_7 are not listed since no operating data are available for these parameters. Note that there are three different operating points at a mass flow of about 20 kg/s, resulting in different gross powers due to variations in condenser pressure. Fig. 8 illustrates the validation for two important plant performance indicators, the gross power output a) and the working fluid mass flow b) as parity plots. The range for a maximum of 10% deviation is shown in dashed lines. All models match with the operating data reasonably well at the maximum operating point (≈2360 kW and ≈29 kg/s), which is not surprising since the individual component models were designed for this point. For part load conditions, the quality of the models spread quite far. In the case of gross power output, the model in this study, the design point model and Model-5 show promising results with RMSD smaller than 155 kW (see Table 5). The simulated values for these models are almost without exception in the 10% deviation range. The literature model and Model-4 show larger deviations in part load conditions and are outside of the 10% deviation range. This is probably a consequence of the error resulting from determining the condensation pressure. Stodola's law does not seem to predict the turbine outlet pressure very accurately (RMSD in p_8 of 6.4 bar, see Table 6), which results in an underestimation in gross power due to the smaller pressure drop in the turbine. In the case of the working fluid mass flow, the relative deviations are not as large. Along with the model in this study and Model-5, Model-4 matches the operating data very well with the lowest RMSD of 1.09 kg/s. The literature model and the design point model show rather poor predictions for the working fluid mass flow in part load conditions. Table 6 also includes the mean absolute percentage error (MAPE) to compare the quality of the different models. The MAPE is calculated as:

$$\mathrm{MAPE} = \frac{1}{n}\sum_{i=1}^{n}\left|\frac{y_{data} - y_{model}}{y_{data}}\right| \tag{11}$$

In comparison to the RMSD, the MAPE is not scale-dependent and can therefore be used to evaluate the quality of the whole model and not only for single variables. The model in this study and Model-5 obtain the lowest values for the MAPE (see Table 5).

In summary, the evaluation of the models based on the part load operating points does not provide a clear result. Therefore, the

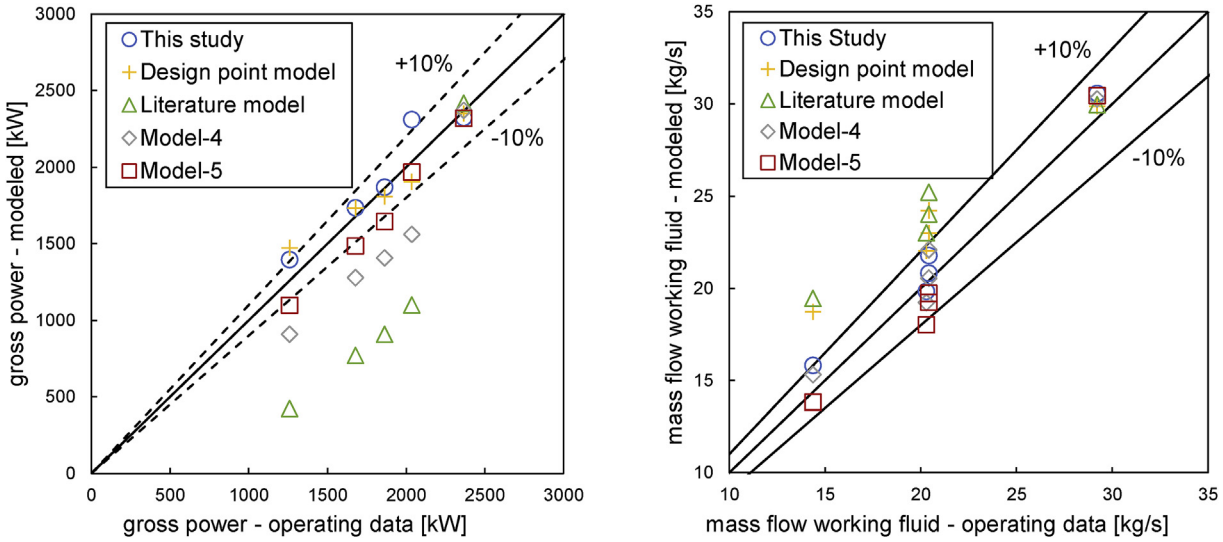

Fig. 8. Validation of the studied models for several stationary operating points for gross power (left) and working fluid mass flow (right).

Table 5
RMSD and MAPE of gross power for the studied models.

	This study	Design point model	Literature model	Model - 4	Model - 5
RMSD [kW]	120	220	717	317	155
MAPE [−]	0.04	0.10	0.39	0.13	0.06

methodology to calculate the annual power yield (see Section 0) is applied to all models in the next section.

7. Calculation of annual power yield

Applying the methodology described in Section 0, the annual gross power yield is calculated for the five part load models studied here. Fig. 9 illustrates the simulated cumulative gross power for the studied models a) and compares those values with the operating data in b). Horizontal segments (slope equals zero) indicate that no electricity is produced. The model developed for this study achieves the smallest difference for the annual power yield. Model-5 and the design point model show reasonably good agreement with operating data, whereby the design point model overestimates and Model-5 underestimates the annual yield. The overestimation by the design point model is probably due to the constant isentropic efficiency, which is too high for most part load conditions. Table 5 summarizes the RMSD between model and operating data for gross power in 2016. These values also prove the quality of the novel developed model in this study, Model-5 and the design point model. Fig. 9 b) allows a more detailed analysis of the quality of the investigated part load models for the different seasons. In the figure, the difference in cumulative power of modeled and operating data is plotted for 2016. A perfect model would therefore lie on the x-axis over the entire time span. Negative values represent an underestimation by the model and positive values an overestimation, respectively. The plot illustrates the poor agreement with operating data of the literature model over the entire year (RMSD of 717 kW). This is the result of the false prediction of the turbine outlet pressure by Stodola's law, which computes turbine outlet pressures that are too high. This is probably the consequence of the non-compliance with the requirements to apply Stodola's law, since the turbine installed in Unterhaching (Germany) is a controlled single-stage turbine. These high outlet pressures in turn lead to reduced pressure differences over the turbine and therefore reduce the gross power output. Model-4 predicts the gross power much better (RMSD of 317 kW). An interesting observation is that Model-4 shows relatively small deviations from operating data during summertime but rather large deviations in spring and fall (indicated by high gradients). This is an effect of the constant condenser pressure in Model-4. The utilization of different pressure levels in Model-5 results in a significant increase in accuracy (RMSD of 155 kW). Compared to Model-4, the gradients in spring and fall are reduced and the match is quite good in summer (almost no gradient). Model-4 and Model-5 both underestimate the produced gross power. Since the only difference between Model-5 and the model in this study is the heat exchanger approach, this underestimation is probably a consequence of the power law approach to calculate the ohtc. Fig. 7 also supports this assumption because the heat exchanger duty is the highest for the EDR approach and increased heat transmission from the brine to the Kalina cycle leads to higher gross powers. The design point model has worse accuracy than Model-5 and the model developed in this study (RMSD of 220 kW) but better accuracy than Model-4. It calculates the gross power reasonably well in winter and overestimates the power output in summer. The good agreement between data and model in winter is a consequence of the maximum operating point, which is somewhat similar to operating conditions in winter. The assumption of a constant isentropic turbine efficiency leads to the overestimation of gross power because this value is not valid in summertime operating conditions. However, the comparable good agreement of the design point model with the operational data is an interesting finding. As mentioned above, the design point model does not account for any part load behavior, but only applies constant values of the isentropic efficiency and the overall heat transfer coefficient. Since this model shows better performance than the part load model based on the literature, the importance of having a validated part load model for the specific plant can be concluded. The accuracy of the design point model would increase further if the main share of the operating time is in the vicinity of the design

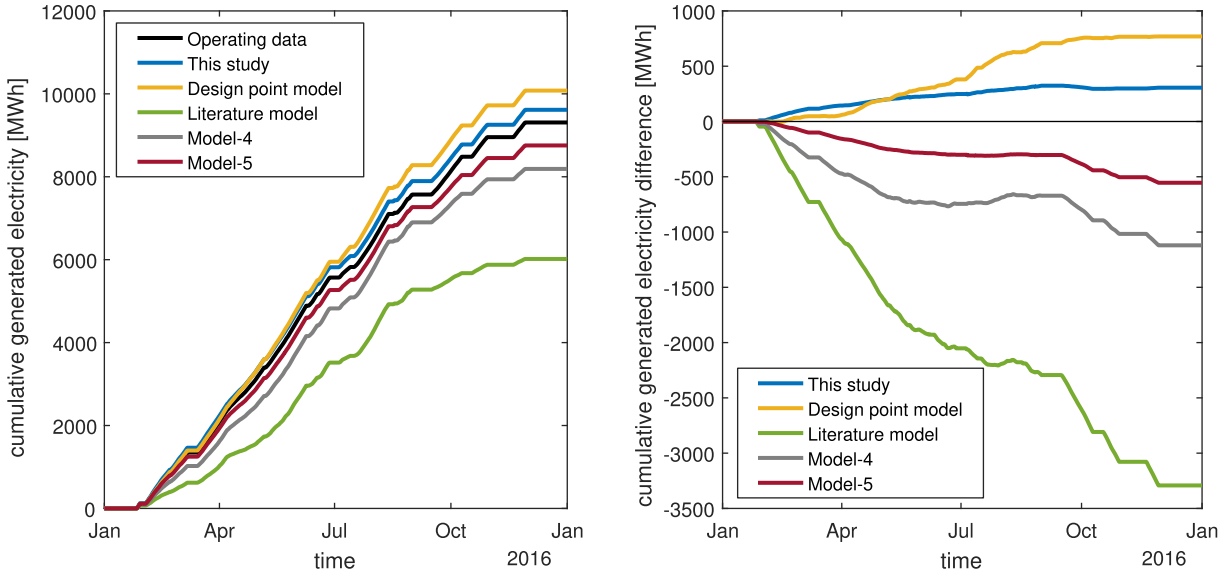

Fig. 9. Simulated cumulative power for the studied part load models (left) and difference between simulated cumulative power and operating data (right).

point. Fig. 10 illustrates the brine mass flow distribution which is available for power production in the KC power plant in Unterhaching (Germany) for 2016.

Fig. 11 compares the modeled and the operating data for gross power by means of a parity plot. For the sake of clarity, the individual data points (about 20k per model) are not plotted, but the envelope around the point cloud, which marks the scatter area of the model, is indicated. However, the areas contain no information about the distribution of the operating points. Therefore, they can only be considered as qualitative comparison criteria. For a quantitative evaluation of the models, refer to the RMSD and MAPE in Table 5. The figure confirms the results discussed above. All models predict the operating data rather well for high power outputs in the vicinity of the maximum operating point. For lower gross powers, only the model of this study, Model-4 and Model-5 show reasonably good agreement between simulated values and operating data, due to the use of the empirical correlation for the turbine efficiency defined in equation (1).

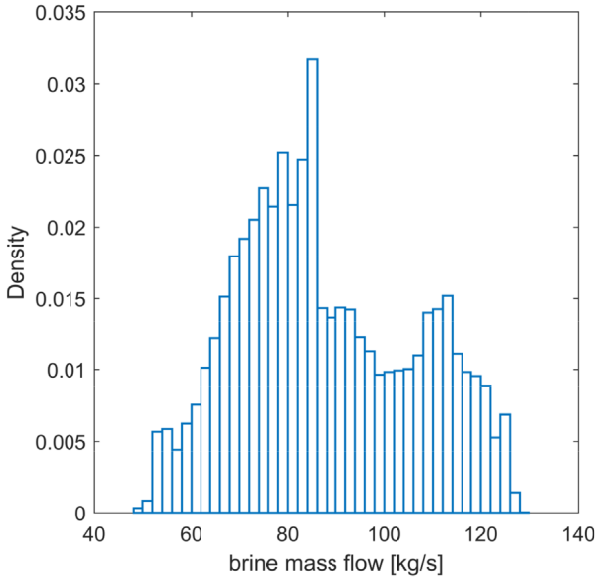

Fig. 10. Distribution of brine mass flow values in 2016.

8. Conclusion

The off-design behavior of power plants is especially important for combined heat and power concepts. Due to the low heat demand in the summer, the energy from geothermal water during this time of the year and the excess geothermal energy in the winter can be utilized to generate power. These power plants are obviously operated under various load conditions, because they have to adapt to the heat demand. Numerical thermodynamic modeling is a very common way of investigating power plants under part load conditions. This paper compares several approaches to simulate the behavior of the Kalina power plant in Unterhaching (Germany) in off-design conditions and validates the models with real operating data from 2016. Different part load models for the two most important components in the cycle, the heat exchangers, and the turbine are investigated. Different approaches to model the isentropic efficiency are presented for the turbine simulation. The turbine outlet pressure, respectively the condensation pressure, is simulated in three ways: Stodola's law, constant pressure, and discretized pressure levels. The heat exchanger models vary greatly in terms of level of detail. The most basic model utilizes constant heat transfer coefficients calculated from a maximum operating point. A more complex model calculates these heat transfer coefficients via a power law approach as a function of the mass flow. The most sophisticated approach simulates the heat exchangers by employing the detailed geometry of the installed plate heat exchangers in the KC in Unterhaching (Germany). Various combinations of these component models are used to simulate the whole power plant. These plant models are then compared to the operating data for the purpose of evaluating them. As evaluation criterion, the RMSD and the MAPE were calculated for several operating points. Furthermore, the annual power yield of the plant is computed and compared to the operating data. The following conclusions can be drawn from this comparison:

1. The implementation of Stodola's law to calculate the turbine pressure outlet has to be done with caution and the assumptions of the approach have to be considered. For example, ORC often

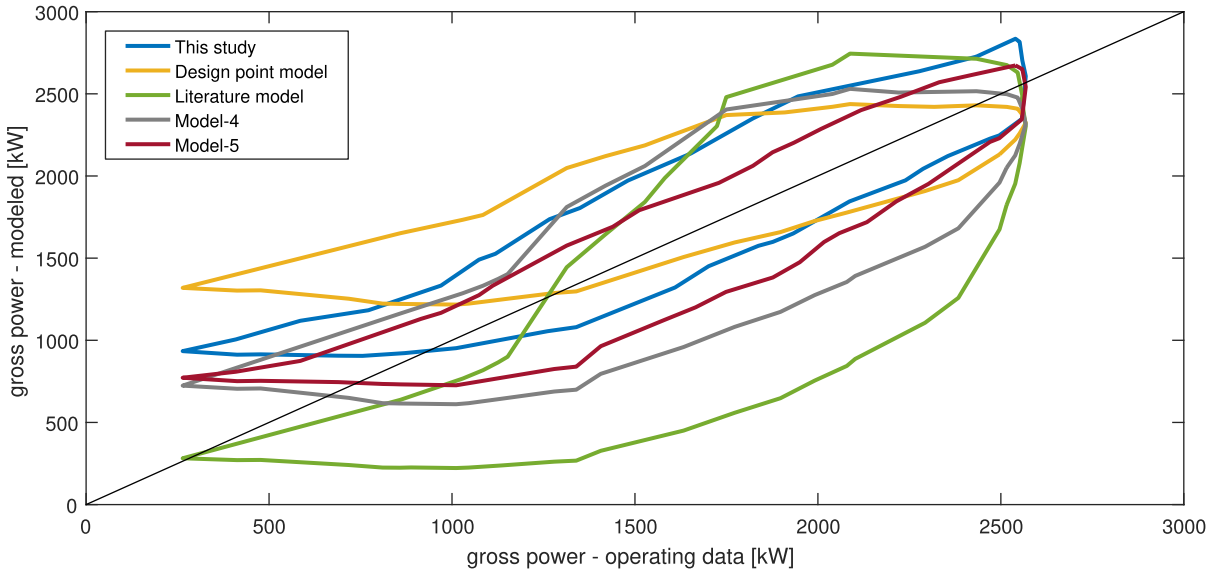

Fig. 11. Comparison of scatter area of the studied models for gross power in 2016.

utilize single-stage turbines because the enthalpy difference of the organic working fluids in preheating, evaporation, superheating, and expansion is lower than compared to water [36]. However, Stodola's law is only valid for uncontrolled, multistage turbines.

2. A well-matching correlation for the isentropic efficiency of the turbine is needed to calculate the gross power output. Therefore, a function of mass flow and turbine outlet pressure seems promising.
3. Heat exchanger modeling with a power law approach to calculate the heat transfer coefficient yields rather accurate results. For plate heat exchangers, an exponent of approx. 1.1 was derived from the operating data for the ammonia-water mixture.
4. The implementation of the detailed plate geometry in the EDR tool allows for very accurate results. However, the method is numerically expensive and the geometry data is required, which commonly is a manufacturing secret.
5. The modeling approach with constant efficiencies and heat transfer coefficients, taken from a design point, is rather easy to implement and achieves good accuracy in the vicinity of the design point. It is a feasible approach to simulate part load behavior if the load conditions of the simulated plant do not vary too much. A distribution plot (see Fig. 10) could visualize this. Furthermore, the design point approach is suitable if only less information about the specific components is known. In that case, it is worth using this approach instead of the models used in the literature.

Acknowledgements

The authors would like to sincerely thank *Geothermie Unterhaching GmbH & Co KG* for providing operating data for the Kalina power plant in Unterhaching (Germany). Funding from the Bavarian State Ministry of Education, Science and the Arts in the frame of the project Geothermie-Allianz Bayern is gratefully acknowledged.

Nomenclature

Acronyms and abbreviations

CHP	combined heat and power
EDR	Aspen Exchanger Design and Rating
ohtc	overall heat transfer coefficient
KC	Kalina cycle
LMTD	logarithmic mean temperature difference
MAPE	mean absolute percentage error
ORC	Organic Rankine Cycle
RMSD	root mean square deviation

Subscripts and superscripts

corr	correlation
D	design point
ex	exchange
eva	evaporator
in	inlet
lm	logarithmic mean
out	outlet
s	isentropic
MP	maximum operating point
T	turbine

Variables

Δ	Difference, –
η	Efficiency, –
ρ	Density, kg/m3
a	Correlation parameter, –
A	Area, m2
h	Specific enthalpy, J/kgK
$\dot{m}$	Mass flow, kg/s
n	Number of data points
p	Pressure, bar
$\dot{Q}$	Heat flow, W
T	Temperature, K
U	Overall Heat transfer coefficient, W/m2K
x	Vapor quality, –

Appendix

The operating data for the operating points used for the validation are provided here. In addition, the RMSD and MAPE of the studied models are summarized for the corresponding values.

Table 6
Measurement data of the maximum operating point and some other part load points with corresponding RMSD and MAPE of the studied models.

		P_T	$\dot{m}_1$	$\dot{m}_4$	T_1	T_2	T_3	T_4	T_5	T_6	T_7	T_8	T_9	T_{10}	p_1	p_2	p_3	p_4	p_5	p_6	p_7	p_8	p_9	p_{10}	$\dot{m}_A$	T_A	p_A
	Units	kW	kg/s	kg/s	°C	°C	°C	°C	°C	°C	°C	°C	°C	°C	bar	bar	bar	bar	bar	bar	bar	bar	bar	bar	kg/s	°C	bar
Operating point	Maximum	2364	29.21	28.42	27	58	120	119	n.a.	120	n.a.	94	48	24.40	20.35	20.04	18.96	18.70	8.82	18.88	n.a.	8.65	8.42	8.36	122	124	9.11
	1	1678	20.29	19.20	22	58	120	120	n.a.	120	n.a.	90	47	18.87	19.76	19.36	18.28	18.15	7.29	18.20	n.a.	7.03	6.87	6.86	80	124	8.51
	2	1863	20.42	19.49	19	57	120	120	n.a.	120	n.a.	88	45	16.47	19.77	19.38	18.25	18.11	6.71	18.16	n.a.	6.45	6.24	6.19	84	124	8.98
	3	2035	20.42	19.78	15	57	121	121	n.a.	121	n.a.	87	42	12.93	19.65	19.42	18.85	18.73	6.42	18.80	n.a.	6.29	6.14	6.13	91	124	8.69
	4	1260	14.36	13.98	13	56	120	120	n.a.	120	n.a.	84	40	11.60	19.36	19.15	18.87	18.81	6.01	18.83	n.a.	5.89	5.82	5.81	64	124	8.32
RMSD (units: same as variables)	this work	141	1.12	0.60	3.43	4.84	0.58	0.43	n.a.	0.52	n.a.	3.32	8.78	1.64	1.06	0.76	0.31	0.36	0.27	0.34	n.a.	0.30	0.32	0.34	—	—	—
	design point model	117	2.96	2.44	6.45	1.18	0.58	0.43	n.a.	0.52	n.a.	5.34	6.40	7.56	0.65	0.64	0.31	0.36	2.02	0.34	n.a.	2.03	1.95	1.92	—	—	—
	literature model	814	3.74	3.17	19.70	1.70	0.58	0.43	n.a.	0.52	n.a.	18.82	10.36	21.24	0.65	0.64	0.31	0.36	6.38	0.34	n.a.	6.40	6.32	6.29	—	—	—
	model-4	378	1.09	0.70	6.45	1.08	0.58	0.44	n.a.	0.52	n.a.	6.20	3.70	7.55	0.58	0.65	0.32	0.37	2.02	0.35	n.a.	2.03	1.95	1.92	—	—	—
	model-5	153	1.32	1.45	3.90	1.35	0.58	0.43	n.a.	0.52	n.a.	2.99	6.03	2.10	0.58	0.65	0.32	0.37	0.27	0.35	n.a.	0.30	0.34	0.37	—	—	—
MAPE [–]	this work	0.06	0.05	0.03	0.17	0.08	0.00	0.00	n.a.	0.00	n.a.	0.03	0.19	0.08	0.05	0.04	0.02	0.01	0.03	0.02	n.a.	0.04	0.04	0.05	—	—	—
	design point model	0.06	0.15	0.12	0.36	0.02	0.00	0.00	n.a.	0.00	n.a.	0.05	0.14	0.48	0.03	0.03	0.02	0.01	0.27	0.02	n.a.	0.28	0.28	0.27	—	—	—
	literature model	0.44	0.19	0.16	1.11	0.02	0.00	0.00	n.a.	0.00	n.a.	0.19	0.22	1.35	0.03	0.03	0.02	0.01	0.87	0.02	n.a.	0.89	0.90	0.90	—	—	—
	model-4	0.20	0.05	0.03	0.36	0.02	0.00	0.00	n.a.	0.00	n.a.	0.06	0.07	0.48	0.03	0.03	0.02	0.01	0.27	0.02	n.a.	0.28	0.28	0.27	—	—	—
	model-5	0.08	0.06	0.07	0.20	0.02	0.00	0.00	n.a.	0.00	n.a.	0.03	0.13	0.12	0.03	0.03	0.02	0.01	0.03	0.02	n.a.	0.04	0.05	0.05	—	—	—

References

[1] Agemar T, Weber J, Schulz R. Deep geothermal energy production in Germany. Energies 2014;7(7):4397–416.
[2] GeotIS. The geothermal information system for Germany [January 03, 2018]; Available from: www.geotis.de/.
[3] Eyerer S, Hofbauer S, Schifflechner C, Wieland C, Spliethoff H. Study on the power generation from hydrothermal geothermal energy: potential of geothermal energy in the German energy system. BWK - Energie-Fachmagazin 2017;(10):47–50.
[4] Zhang X, He M, Zhang Y. A Review of research on the Kalina cycle. Renew Sustain Energy Rev 2012:5309–18.
[5] Campos Rodríguez CE, Escobar Palacio J Carlos, Venturini O, Lora E, Cobas V, Santos D, et al. Exergetic and economic comparison of ORC and Kalina cycle for low temperature enhanced geothermal system in Brazil. Appl Therm Eng 2013;52:109–19.
[6] Köhler Silke. Geothermisch angetriebene dampfkraftprozesse: doctoral thesis. Technische Universität Berlin; 2005.
[7] Thorin Eva. Power cycles with ammonia-water mixtures as working fluid: doctoral thesis. Royal Institute of Technology Stockholm; 2000.
[8] DiPippo R. Second Law assessment of binary plants generating power from low-temperature geothermal fluids. Geothermics 2004;33:565–86.
[9] Walraven D, Laenen B, D'haeseleer W. Comparison of thermodynamic cycles for power production from low-temperature geothermal heat sources. Energy Convers Manag 2013;(66):220–33.
[10] Wieland C, Meinel D, Eyerer S, Spliethoff H. Innovative CHP concept for ORC and its benefit compared to conventional concepts. Appl Energy 2016;183:478–90.
[11] Heberle F, Schifflechner C, Brüggemann D. Life cycle assessment of Organic Rankine Cycles for geothermal power generation considering low-GWP working fluids. Geothermics 2016;64:392–400.
[12] Gabbrielli R. A novel design approach for small scale low enthalpy binary geothermal power plants. Energy Convers Manag 2012;(64):263–72.
[13] Jüdes M, Vigerske S, Tsatsaronis G. Optimization of the design and partial-load operation of power plants using mixed-integer nonlinear programming. In: Pardalos PM, Kallrath J, Rebennack S, Scheidt M, editors. Optimization in the energy industry. first ed. Springer-Verlag; 2009. p. 193–220.
[14] Aspen technology inc. AspenPlus; 2001.
[15] The MathWorks I. MATLAB R2016b. 2017.
[16] Kalina A. Generation of energy by means of a working fluid, and regeneration of a working fluid: United States Patent 4346561; 1982See Suggestions/replace option.
[17] Kalina AI. Combined cycle and waste heat recovery power systems based on a novel thermodynamic energy cycle utilizing low-temperature heat for power generation. In: 1983 joint power generation conference: GT papers. ASME; 1983. V001T02A003.
[18] Kalina AI. Combined-cycle system with novel bottoming cycle. J Eng Gas Turbines Power 1984;106(4):737.
[19] Geothermie unterhaching GmbH & Co KG. [January 08, 2018]; Available from: www.geothermie-unterhaching.de
[20] Zarrouk SJ, Woodhurst BC, Morris C. Silica scaling in geothermal heat exchangers and its impact on pressure drop and performance: wairakei binary plant, New Zealand. Geothermics 2014;51:445–59.
[21] Calise F, Capuano D, Vanoli L. Dynamic simulation and exergo-economic optimization of a hybrid solar-geothermal cogeneration plant. Energies 2015;(8):2606–46.
[22] Wang J, Wang J, Dai Y, Zhao P. Assessment of off-design performance of a Kalina cycle driven by low-grade heat source. Energy 2017;138:459–72.
[23] Yoon SY, Kim MJ, Kim IS, Kim TS. Comparison of micro gas turbine heat recovery systems using ORC and trans-critical CO_2 cycle focusing in off-design performance. Energy Procedia 2017;129:987–94.
[24] Cooke DH. On prediction of off-design multistage turbine pressures. J Eng Gas Turbines Power 1985;(107):596–606.
[25] Traupel W. Thermische turbomaschinen: thermodynamisch-strömungstechnische berechnung. fourth ed. Berlin, Heidelberg: Springer Berlin Heidelberg; 2001.
[26] Alshammari F, Karvountzis-Kontakiotis A, Pesiridis A, Giannakakis P. Off-design performance prediction of radial turbines operating with ideal and real working fluids. Energy Convers Manag 2018;171:1430–9.
[27] Du Y, Chen K, Dai Y. A study of the optimal control approach for a Kalina cycle system using a radial-inflow turbine with variable nozzles at off-design conditions. Appl Therm Eng 2019;149:1008–22.
[28] Fiaschi D, Manfrida G, Maraschiello F. Design and performance prediction of radial ORC turboexpanders. Appl Energy 2015;138:517–32.
[29] Song J, Gu C-w, Ren X. Parametric design and off-design analysis of organic Rankine cycle (ORC) system. Energy Convers Manag 2016;112:157–65.
[30] Dickes R, Dumont O, Daccord R, Quoilin S, Lemort V. Modelling of organic Rankine cycle power systems in off-design conditions: an experimentally-validated comparative study. Energy 2017;123:710–27.
[31] Zheng Y, Hu D, Cao Y, Dai Y. Preliminary design and off-design performance analysis of an Organic Rankine Cycle radial-inflow turbine based on mathematic method and CFD method. Appl Therm Eng 2017;112:25–37.
[32] STEAG energy services GmbH. Ebsilon Professional; 2016.
[33] Incropera FP. Fundamentals of heat and mass transfer. sixth ed. Hoboken NJ:

Wiley; 2007.
[34] Welty JR. Fundamentals of momentum, heat, and mass transfer. fifth ed. Hoboken, NJ: Wiley; 2008.
[35] Mergner H, Schaber K. Performance analysis of an evaporation process of plate heat exchangers installed in a Kalina power plant. Energy 2018;145:105–15.
[36] Schuster A. Nutzung von Niedertemperaturwärme mit Organic-Rankine-Cycle-Anlagen kleiner Leistung. Dissertation; 2011.